Available online at www.sciencedirect.com
SCIENCE DIRECT®

Journal of the European Ceramic Society 24 (2004) 53–64

www.elsevier.com/locate/jeurceramsoc

Polymer impregnation and pyrolysis (PIP) method for the preparation of laminated woven fabric/mullite matrix composites with pseudoductility

Rulin Dong[a], Yoshihiro Hirata[a,*], Hidekazu Sueyoshi[a], Morihide Higo[b], Yoshimitsu Uemura[b]

[a]*Course of Advanced Nanostructured Materials Science and Technology, Graduate School of Science and Engineering, Kagoshima University, Korimoto, Kagoshima 890-0065, Japan*
[b]*Department of Applied Chemistry and Chemical Engineering, Kagoshima University, Korimoto, Kagoshima 890-0065, Japan*

Received 11 September 2002; received in revised form 4 March 2003; accepted 7 March 2003

Abstract

An ethylalcohol solution containing $Si(OC_2H_5)_4$ and $Al(NO_3)_3$ with a composition of mullite, $3Al_2O_3{\cdot}2SiO_2$, was infiltrated into a porous laminated woven fabric of 22–35 vol.% SiC or Al_2O_3–SiO_2 fibers and 8–42 vol.% mullite powder (filler). The solution was then decomposed at 500 °C in air. This polymer impregnation and pyrolysis method (PIP) was repeated 20–23 times to produce a laminated mullite matrix composite of 73–79% density. The pseudoductility of the densified composite when tested in four-point bend was caused by delamination cracks. This mechanical property was enhanced by (1) good dispersion of the mullite filler in the filament yarn, (2) large amounts of dispersed filler, (3) formation of weak bonds in the filament yarn from the pyrolysis of the mullite precursor, and (4) lower amounts of mullite precursor-derived amorphous solid. The infiltration of the mullite filler dispersed electrosterically in an aqueous solution into the woven fabric offered significant pseudoductility, but infiltration of the filler dispersed in the ethylalcohol solution of the mullite precursor resulted in a brittle composite.

Keywords: Composites; Fracture; Mullite; SiC; Suspensions

1. Introduction

Continuous fiber-reinforced ceramic matrix composites (CFCCs) can display high damage tolerance with pseudoductility and may be applied in high temperature structural material applications such as aircraft engine components or spacecraft engine parts. The development of mechanically reliable composites requires a weak chemical bond between the fibers and the matrix to enhance fiber-bridging and fiber-pullout during crack propagation. The main crack in the matrix confronts the high-strength fibers and is deflected along fiber/matrix interfaces. With an increase of applied load, the fibers bridge over the extended crack. Further increase of load causes the fracture and pullout of fibers in the matrix, producing the pseudoductility.[1–11]

CFCCs are divided into the following three types: nonoxide fibers/nonoxide matrix, nonoxide fibers/oxide matrix, and oxide fibers/oxide matrix. Amorphous C and BN are used as interphase materials because of their lubricant property, which enhances the pullout of fibers in SiC/SiC and oxide/oxide composites.[12–17] Recently, oxide interphases such as $LaPO_4$,[18–23] hexaaluminate[24–26] or ZrO_2[27–29] have been studied because of their high stability at high temperatures in an oxidizing environment. The debonding length of fibers in pullout depends on the roughness of the fiber surface, the strength of the fibers and the residual stresses around the interfaces resulting from the difference of thermal expansion coefficient and Young's modulus between the fibers and matrix.[30–34] The introduction of the interphase affects the residual stresses, the chemical

* Corresponding author. Tel.: +81-99-285-8325; fax: +81-99-257-4742.
E-mail address: hirata@apc.kagoshima-u.ac.jp (Y. Hirata).

0955-2219/03/$ - see front matter © 2003 Elsevier Ltd. All rights reserved.
doi:10.1016/S0955-2219(03)00127-4

reaction at the interfaces, the roughness of the fibers and the resultant pseudoductility.[35,36]

The matrix phase of CFCCs is usually fabricated by netshape or near-netshape processing such as chemical vapor infiltration (CVI),[17,37,38] polymer impregnation and pyrolysis (PIP)[39–41] or reaction sintering (RS).[42,43] The CVI and RS processes offer a dense matrix but the PIP process leaves residual pores. Although PIP takes a longer processing time than CVI or RS, it has advantages in (1) the low temperature processing and (2) the use of simple processing equipment (low cost). The structure of composites processed by the PIP method is analogous to that of a concrete material. The fibers, the ceramic powder filler and the precursor polymer in the PIP process correspond to the steel bars, rock and sand, and cement in the concrete material, respectively. In our previous paper,[39] a polytitanocarbosilane/xylene solution was impregnated into a porous Si–Ti–C–O fiber/mullite filler composite and decomposed at 1000 °C in an Ar atmosphere. The PIP sequence was repeated 8 times to produce a layered composite with 90% density. This composite showed a significant pseudoductility with a maximum deformation strength of 290 MPa in bend. Based on the above successful PIP process, we studied the processing, microstructure and mechanical properties of layered composites formed form continuous fibers (SiC, aluminosilicate)/mullite powder/mullite precursor solution by the PIP process at 500 °C in air. In this processing, no interphase material was introduced.

2. Experimental procedure

2.1. Mullite precursor solution

$Al(NO_3)_3{\cdot}9H_2O$ (purity > 98.0 mass%, Wako Pure Chemical Industries, Ltd., Japan) and $Si(OC_2H_5)_4$ (purity > 95.0 mass%, Wako Pure Chemical Industries, Ltd., Japan) were used to prepare a mullite precursor solution. In the PIP process, a high ceramic yield of solids-to-polymer, a high concentration and a low viscosity are desired for the precursor solution in order to eliminate the open pores in the green composite after a small number of PIP sequences. $Al(NO_3)_3{\cdot}9H_2O$ was dissolved in ethylalcohol (purity > 99.5 vol.%) at 80 °C and cooled to adjust the concentration to 2 M. The $Al(NO_3)_3$ ethanol solution was mixed with a 2 M-$Si(OC_2H_5)_4$ ethanol solution at a molar ratio of Al/Si = 3/1 to provide a decomposition product of mullite composition. The similar composition for the aluminosilicate fibers, the mullite filler and the mullite matrix formed from the precursor solution, reduces the residual stresses caused by the cooling after processing. The mixed solution was refluxed at 80–83 °C to accelerate partial hydrolysis. Fig. 1 shows the viscosity of the mullite precursor solution as a function of reflux time. The viscosity gradually increased up to 1.5 h of reflux and then rapidly increased at longer times due to the polymerization of the solution. A low viscosity mullite precursor solution refluxed for 1 h was chosen to be impregnated into the porous green composite. After the reflux of the precursor solution for 1 h at 80–83 °C, the solvent was evaporated by heating the solution at 100 °C for 72 h, producing a white residue. The thermal decomposition behavior of the derived solid was analyzed with thermogravimetric differential thermal analysis (TG-DTA) at a heating rate of 10 °C/min to 1000 °C in air (Thermoflex, Rigaku Co., Tokyo, Japan). The phase identification of the heated solid was conducted using X-ray diffractometry (XRD, Model No. 2013, Rigaku Co., Tokyo, Japan) and the specific surface area of the heated powder was measured by the BET method (Micromeritics Flow Sorb II 2300, Shimadzu Co., Japan).

2.2. Green laminated composite

The starting materials used for the preparation of green composites are listed in Table 1. As-received sol-gel-processed crystalline mullite powder shown in Fig. 2, consisted of flaky particles with a size distribution of 0.7–3.8 μm (specific surface area 5.7 m^2/g). The micrometer-sized mullite particles were inserted as filler into the open spaces between the continuous fibers. Fig. 3 shows the flow chart for the preparation of green laminated composites. Two kinds of mullite suspensions were prepared for infiltration into the laminated fabric sheets. One is an aqueous mullite suspension with 46.1 vol.% solid and polyacrylicammonium dispersant (PAA, average molecular weight 10 000) of 0.6 mass% against the mass of the mullite. The pH of the suspen-

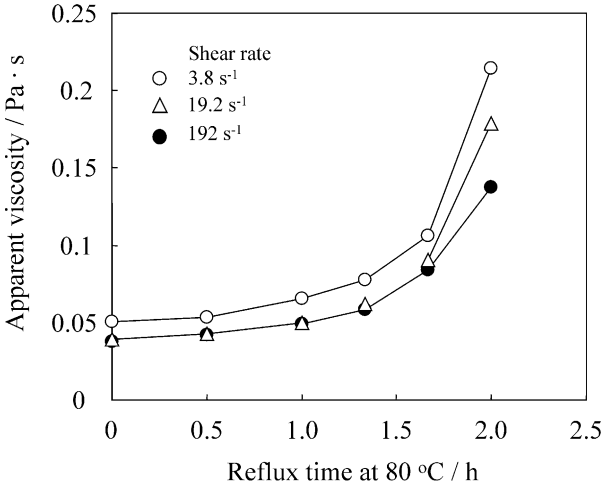

Fig. 1. Apparent viscosity of the mullite precursor alcohol solution prepared from 2 M-$Al(NO_3)_3$ and 2 M-$Si(OC_2H_5)_4$, as a function of reflux time at 80 °C.

Table 1
Characteristics of raw materials used for the preparation of layered woven fabric/mullite matrix composites

	Fibers		Mullite powder (filler)
	SiC satin	Aluminosilicate fabric	
Chemical composition (mass%)	69.3 Si, 29.6 C, 0.6 Al, 0.5 O	85 Al_2O_3, 15 SiO_2	71.80 Al_2O_3, 28.05 SiO_2, 0.30 ZrO_2, 0.10 TiO_2, 0.01 Na_2O
Yarn	1600 filament	1000 filament	
Young's modulus (GPa)	397	210	
Tensile strength (GPa)	2.84	2.0	
Diameter (μm)	7.5	15	1.75 (cumulative partical size distribution: 0.65 μm/10%, 1.75 μm/50%, 3.75 μm/90%)
Specific surface area (m^2/g)			5.7
Density (g/cm^3)	3.24	3.23	3.16

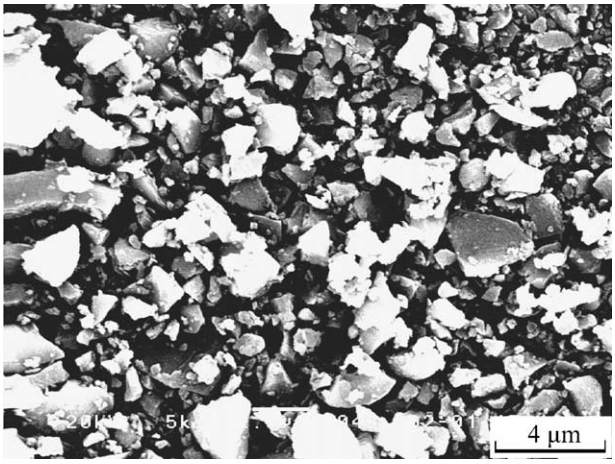

Fig. 2. Scanning electron micrograph of as-received sol-gel-processed mullite powder.

sion was adjusted to 9–10 using 1.0 M-NH_4OH solution to enhance the dispersion of the negatively charged mullite particles by electrosteric stabilization. Another suspension was prepared by mixing the mullite particles at 10 and 30 vol.% solids with the refluxed mullite precursor solution. All the suspensions were stirred for 24 h at room temperature. SiC satin (219 μm thick, 25 mm wide and 38 mm long) assembly of 10 sheets or Al_2O_3–SiO_2 fabric (325 μm thick, 25 mm wide, and 38 mm long) assembly of 8 sheets were laminated together in the aqueous mullite suspensions or mullite precursor suspensions, under a pressure of 9.8 kPa. The green laminated composites consolidated from the aqueous mullite suspensions or mullite precursor suspensions were calcined for 1 h at 1000 °C or for 30 min at 500 °C, respectively, in air or in an Ar atmosphere. The characteristics of the laminated composites are shown in Table 2. The fraction of mullite powder filler in the composite became higher as the solid concentration of the suspension increased. The fiber fraction was in the range of 22–35 vol.%. The formation of the solid derived from the mullite precursor solution is described in the next section.

2.3. PIP process with mullite precursor solution and mechanical properties of densified composite

The mullite precursor solution was infiltrated into the green laminated composites of the SiC satin-mullite filler system and the Al_2O_3–SiO_2 fabric–mullite filler system, and decomposed by heating at 500 °C for 30 min in air. This PIP sequence was repeated 20–23 times to reduce the porosity. After the 15th PIP sequence, the composites with Al_2O_3–SiO_2 fabric and SiC satin were heated at 1000 °C for 1 h in air and an Ar atmosphere, respectively, to densify the matrix formed from the mullite precursor solution. Then, the PIP sequence was resumed for 5–8 times with the heat-treatment at 500 °C in air. After 20–23 PIP sequences, the composites were again heat-treated at 1000 °C for 2 h in air or in an Ar atmosphere. The density of the PIP-processed composite was measured by the Archimedes method, using distilled water. The microstructure of the densified composites was observed by optical microscopy and

Table 2
Phase compositions of the laminated composites after 20–23rd PIP sequences

Sample	Fiber	Mullite powder suspension	Satin or fabric (vol.%)	Mullite powder (vol.%)	Mullite precursor-derived solid (vol.%)	Pore	
						Open (vol.%)	Closed (vol.%)
No. 1	SiC	46 vol.% aqueous	21.96	41.75	10.74	22.13	3.42
No. 2	Al_2O_3–SiO_2	46 vol.% aqueous	32.66	35.76	9.72	16.69	5.17
No. 3	Al_2O_3–SiO_2	10 vol.% mullite precursor	34.52	7.60	31.30	20.99	5.59
No. 4	Al_2O_3–SiO_2	30 vol.% mullite precursor	28.37	23.09	27.52	15.40	5.62

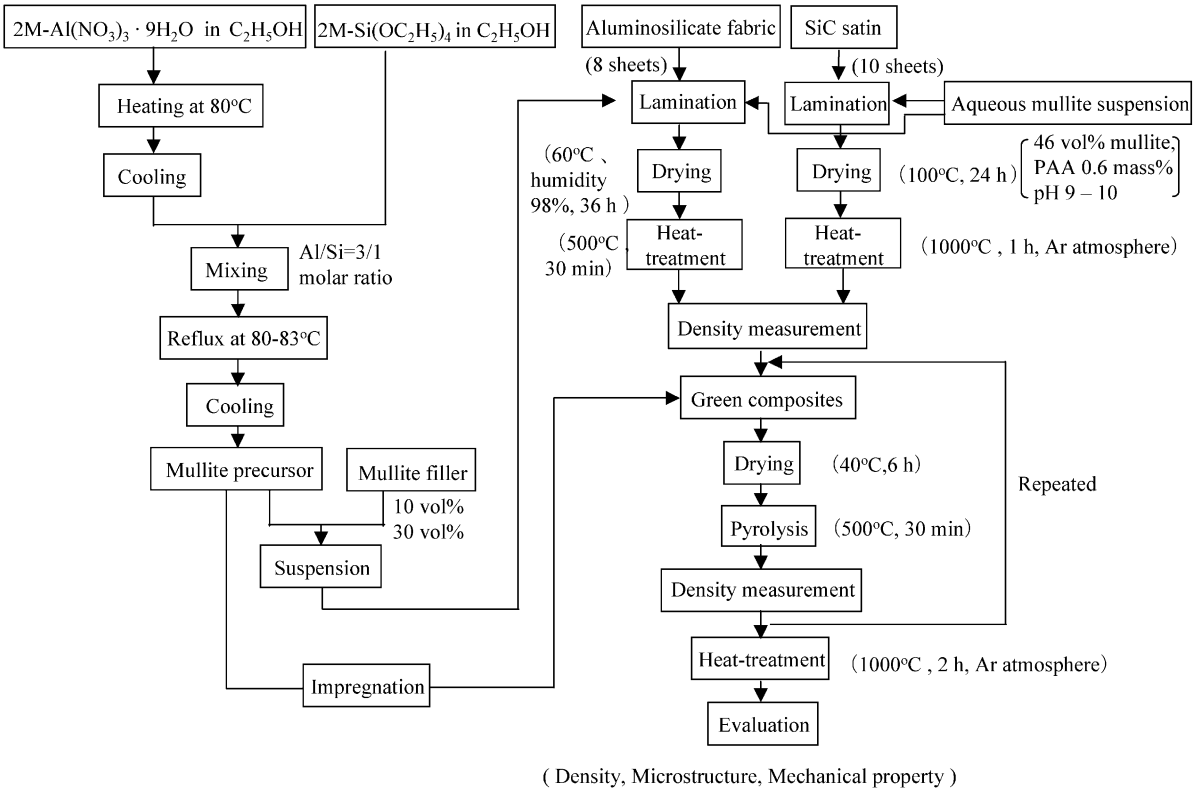

Fig. 3. Flow chart of the preparation of laminated green composites of alumino-silicate fabric and SiC satin.

scanning electron microscopy (Model No. SM300, Topcon Technologies, Inc., Japan). The composites were cut by a diamond wheel into test specimens 4 mm wide, 3 mm high and 38 mm long. To avoid damage to the fabric from polishing, the flexural strength was measured with as-cut specimens. The flexural strength was measured at room temperature in four-point bend over a 10 mm upper span and 30 mm lower span at a crosshead speed of 0.5 mm/min (Model UTM-1-5000 BE, Toyo Baldwin Co., Japan). A strain gauge was attached to the tensile surface during the measurement of flexural strength.

3. Results and discussion

3.1. Thermal properties of the mullite precursor

Fig. 4(a) and (b) shows the TG and DTA curves, respectively, for $Al(NO_3)_3{\cdot}9H_2O$, for silica gel derived from $Si(OC_2H_5)_4$ by the hydrolysis with HCl catalyst, and for the mullite precursor produced from $Si(OC_2H_5)_4$ and $Al(NO_3)_3$, dried at 100 °C for 72 h in air. The weight loss of $Al(NO_3)_3{\cdot}9H_2O$ due to its pyrolysis is calculated to be 86.4% ($Al(NO_3)_3{\cdot}9H_2O \rightarrow 1/2Al_2O_3 + 3NO_2 + 3/4O_2 + 9H_2O$). The experimental result showed a smaller weight loss of 55.8% at 600 °C. The difference in the weight loss indicates a partial decomposition of $Al(NO_3)_3{\cdot}9H_2O$ with its melting point of 73 °C during the earlier drying at 100 °C. A chemical composition of $Al(OH)_2NO_3$ was estimated for the dried $Al(NO_3)_3{\cdot}9H_2O$, because the calculated weight loss (58.6%, $Al(OH)_2NO_3 \rightarrow 1/2Al_2O_3 + NO_2 + 1/4O_2 + H_2O$) is then close to the measured value. The mullite precursor and the dried $Al(NO_3)_3$ showed similar DTA curves upon heating to 400 °C, indicating that $Al(OH)_2NO_3$ coexisted with silica in the mullite precursor. As seen in Fig. 4(b), an exothermic peak was measured at about 900 and 980 °C for dried $Al(NO_3)_3$ and the mullite precursor, respectively. These exothermic peaks were associated with the crystallization of γ-Al_2O_3 phase, as confirmed by the XRD patterns of the heated powders. The silica component coexisting with the Al_2O_3 component shifted the crystallization of the γ-alumina phase to higher temperature. A similar result was also observed upon heating in an Ar atmosphere for the system $Al(NO_3)_3$, silica gel and mullite precursor. Fig. 5 shows the X-ray diffraction patterns of the phases produced in the mullite precursor heated for 2 h at 500–1300 °C in an Ar atmosphere. The precursor changed to γ- and α-alumina at 1000–1150 °C. The crystallization of mullite occurred at temperatures above 1200 °C with the disappearance of γ-alumina. No formation of a crystalline silica phase at temperatures below 1150 °C occurred, indicating that mullite was formed through the reaction between γ-alumina and

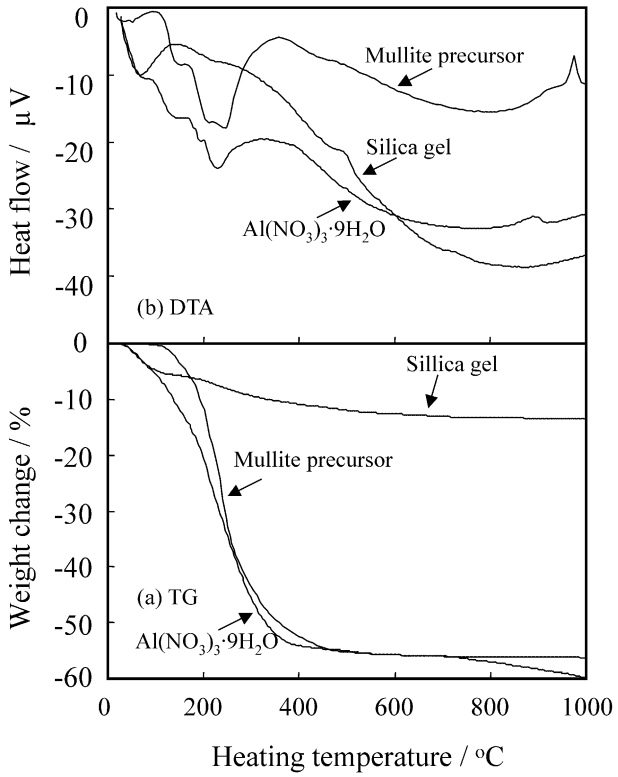

Fig. 4. TG (a) and DTA (b) curves for $Al(NO_3)_3$, silica gel derived from $Si(OC_2H_5)_4$ and the mullite precursor produced from $Al(NO_3)_3$ and $Si(OC_2H_5)_4$, with heating in air.

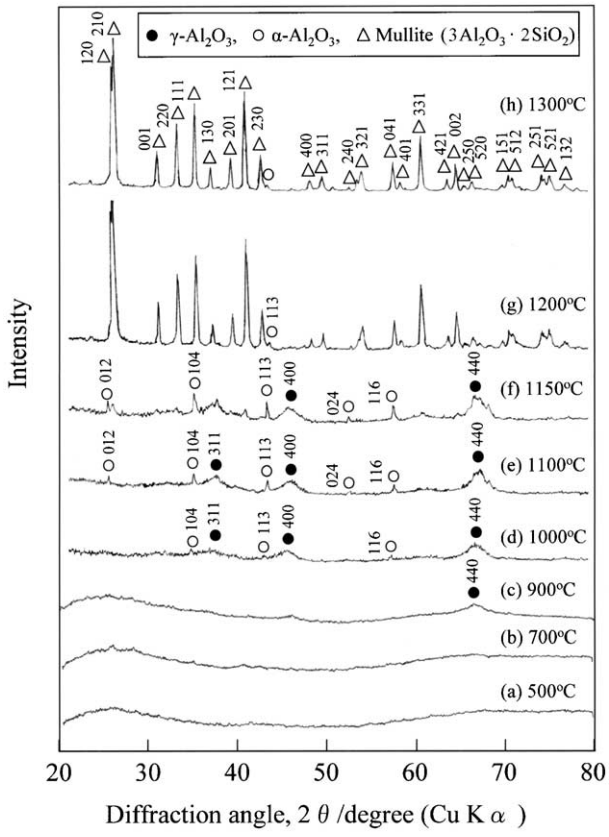

Fig. 5. X-ray diffraction patterns of the phases produced in the mullite precursor heated for 2 h at 500–1300 °C in an Ar atmosphere.

amorphous silica. A similar result for the crystallization of the mullite precursor was observed upon heating in air. The mullite formation was enhanced at 1150 °C in air. As seen in Fig. 5, a trace of α-alumina coexisted with mullite at 1200–1300 °C, suggesting the formation of a SiO_2-rich mullite solid solution.[44] The true density of the heated mullite precursor, which was measured by pycnometer using distilled water, was 2.35±0.01, 2.77±0.01 and 3.09±0.06 g/cm^3 after heating at 500, 1000 and 1300 °C in air, respectively. The increase of powder density is accompanied by shrinkage of powder volume. The volume shrinkage with heating from 500 to 1000 °C was calculated to be 15.3%. Fig. 6 shows the specific surface area of the mullite precursor with heating at 500–1300 °C in air. The specific surface area decreased significantly with the formation of crystalline phases at temperatures above 900 °C. The specific surface area (S) depends on the powder density (ρ) and particle diameter (D) as follows: $S = 6/\rho D$. The diameter of the equivalent spherical mullite precursor particles was calculated to be 19, 414 and 1881 nm after heating at 500, 1000 and 1300 °C, respectively. Therefore, Fig. 6 suggests that the volume of each mullite precursor particle shrunk with heating but rapid grain growth occurred upon the crystallization of the amorphous mullite precursor. In other words, the shrinkage of particle volume with increased powder density is accompanied by the coarsening of particles, resulting in the decreased specific surface area.

3.2. Infiltration of mullite particles into woven fabric

Fig. 7 shows the apparent viscosity as a function of shear rate for the aqueous mullite suspension with 46.1 vol.% solid and the mullite precursor suspensions with

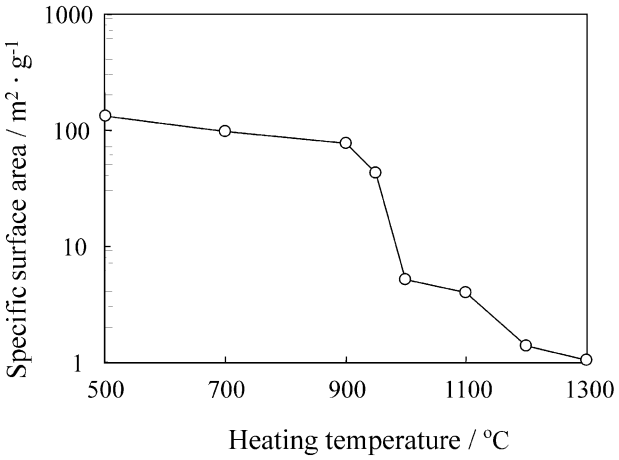

Fig. 6. Specific surface area of the mullite precursor with heating for 2 h at 500–1300 °C in air.

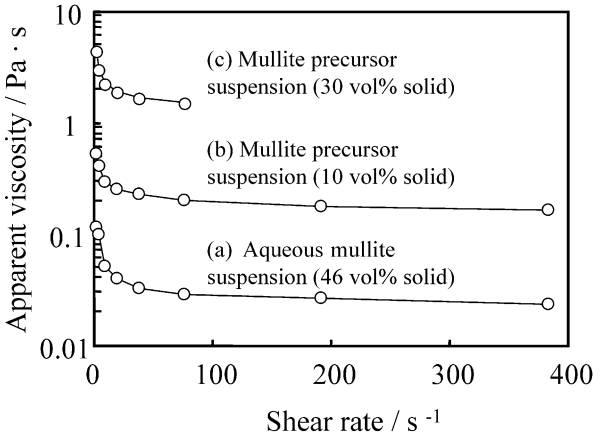

Fig. 7. Apparent viscosity as a function of shear rate for (a) the aqueous mullite suspension with 46.1 vol.% solid and the mullite precursor suspensions with (b) 10 and (c) 30 vol.% mullite powder.

10 and 30 vol.% mullite powder. They both showed pseudoplastic flow. The apparent viscosity decreased in the following order: precursor suspension with 30 vol.% solid > precursor suspension with 10 vol.% solid > aqueous suspension with 46 vol.% solid. The low viscosity of the aqueous suspension is due to the electrosteric stabilization by PAA adsorbed on the mullite particles.[45,46] The high viscosity of the precursor suspension is to be explained by the poor dispersion of mullite particles in the hydrophobic suspension. Fig. 8 shows the microstructures of the SiC satin (a) and aluminosilicate fabric (b,c,d), laminated in the mullite suspensions. In the low viscosity aqueous mullite suspensions [Fig. 8(a) and (b)], the dispersed mullite particles were densely packed between the fibers. In sample 3 laminated in the mullite precursor suspension of 10 vol.% solid [Fig. 8(c)], mullite particles were scarcely observed in the yarn. An increase in the mullite powder content of the precursor suspension [Fig. 8(d)], resulted in the formation of agglomerated mullite filler between the yarn, which was consolidated by the pyrolysis of the mullite precursor at 500 °C. As seen in Table 2, the amount of mullite filler in the laminated green composite depended mainly on the mullite content of the suspension. However, the microstructure of the composite was influenced by the dispersion state of the mullite particles in the suspension and by the viscosity of the suspension.

3.3. PIP process of the mullite precursor solution

In the PIP process, the porosity (P) of open pores in the composite after n sequences is expressed by Eq. (1),

$$P = P_0\left[1 - \frac{1}{1000D_s}\left(\frac{1}{2}C_1M_1 + C_2M_2\right)\right]^n \quad (1)$$

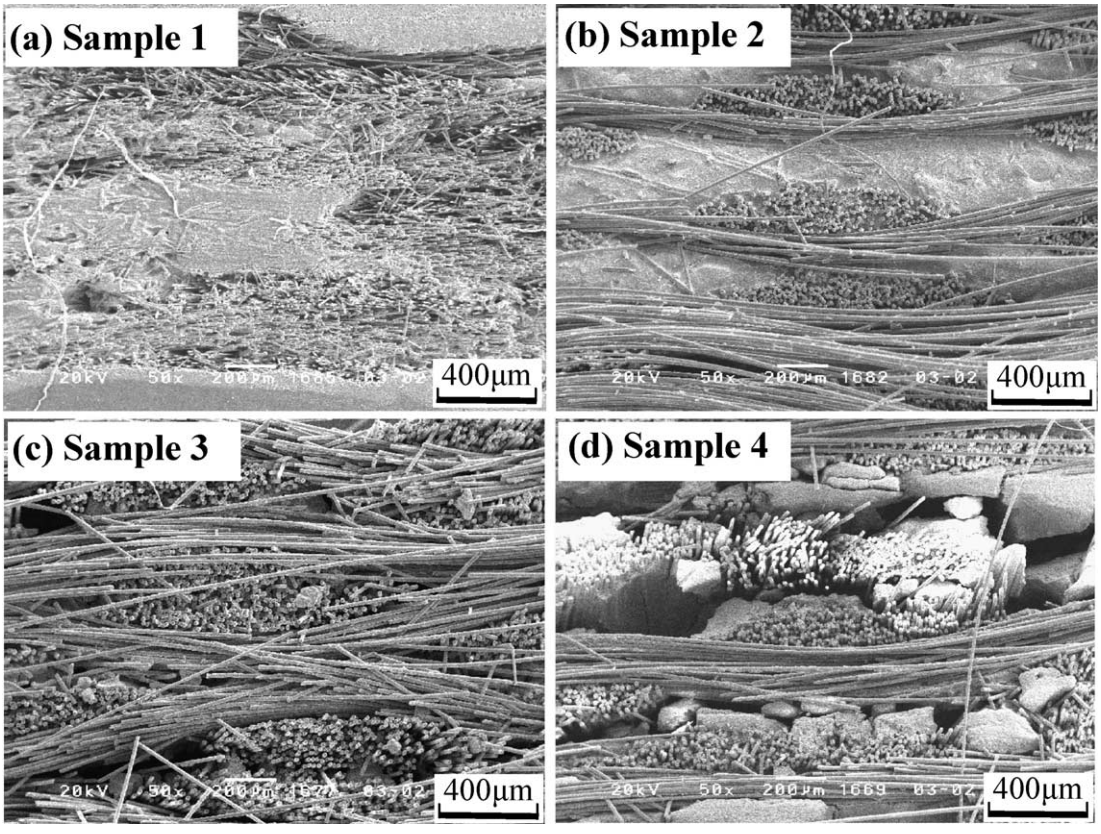

Fig. 8. Microstructures of the SiC satin (a) and aluminosilicate fabric (b,c,d), laminated in the mullite suspensions. See Table 2 for samples.

where P_0 is the initial porosity before the PIP sequences, C_1 (mol/l) the concentration of Al in the mullite precursor solution, M_1 the molecular weight of Al_2O_3, C_2 (mol/l) the concentration of Si in the mullite precursor solution, M_2 the molecular weight of SiO_2, and D_s the density (2.35 ± 0.01 g/cm^3) of the amorphous solid formed from the mullite precursor by the heat treatment at 500 °C in air. Eq. (1) indicates that (1) the porosity decreases gradually with increasing n value, (2) decreased P_0 effectively reduces porosity for a given precursor and (3) a precursor with high C value is desirable for decreasing porosity.

Fig. 9 shows the porosity of the composites as a function of the number of PIP sequences. The solid lines in Fig. 9 represent the porosity calculated by Eq. (1). The increase of porosity at the 15th or 19th PIP sequences is due to the volume shrinkage of the mullite precursor with the increase of heat treatment temperature from 500 to 1000 °C. The measured porosity decreased along the calculated lines. The positive deviation of the measured porosity from the calculated line, represents the decreased elimination efficiency of open pores. A relatively large deviation was observed in sample 1 after the 5th PIP sequence. In this sample, mullite filler at the highest amount (42 vol.%) was dispersed in the woven SiC satin. With the increased number of PIP sequences, the pore channels become quickly constricted, suppressing the subsequent infiltration of mullite precursor. On the other hand, a lower value for the measured porosity than for the calculated porosity indicates a greater disappearance of the open pores than predicted. This result, as shown in sample 4, is explained by the formation of closed pores from open pores during the pyrolysis of the mullite precursor impregnated in the open pores. The formation of closed pores may also occur in the agglomerated mullite filler, observed in Fig. 8(d). Samples 1 and 2, formed from the aqueous mullite suspensions, contained 3–4% closed pores after calcination at 1000 °C and before the PIP process. This type of closed pores remained during the PIP sequences. The further formation of closed pores by the mullite precursor during the PIP sequences was not significant in samples 1 and 2. The final porosity in Fig. 9 was from 21 to 27% (Table 2).

Fig. 10 shows cross sections of the densified composites. Large pores in the range from 100 to 800 μm were observed more in samples 3 and 4 formed from the mullite precursor suspensions than in samples 1 and 2 formed from the aqueous mullite suspensions. The microstructure of the densified composites inherited the uniformity of the green microstructure before the PIP process (Fig. 8). That is, the key factor to achieve a

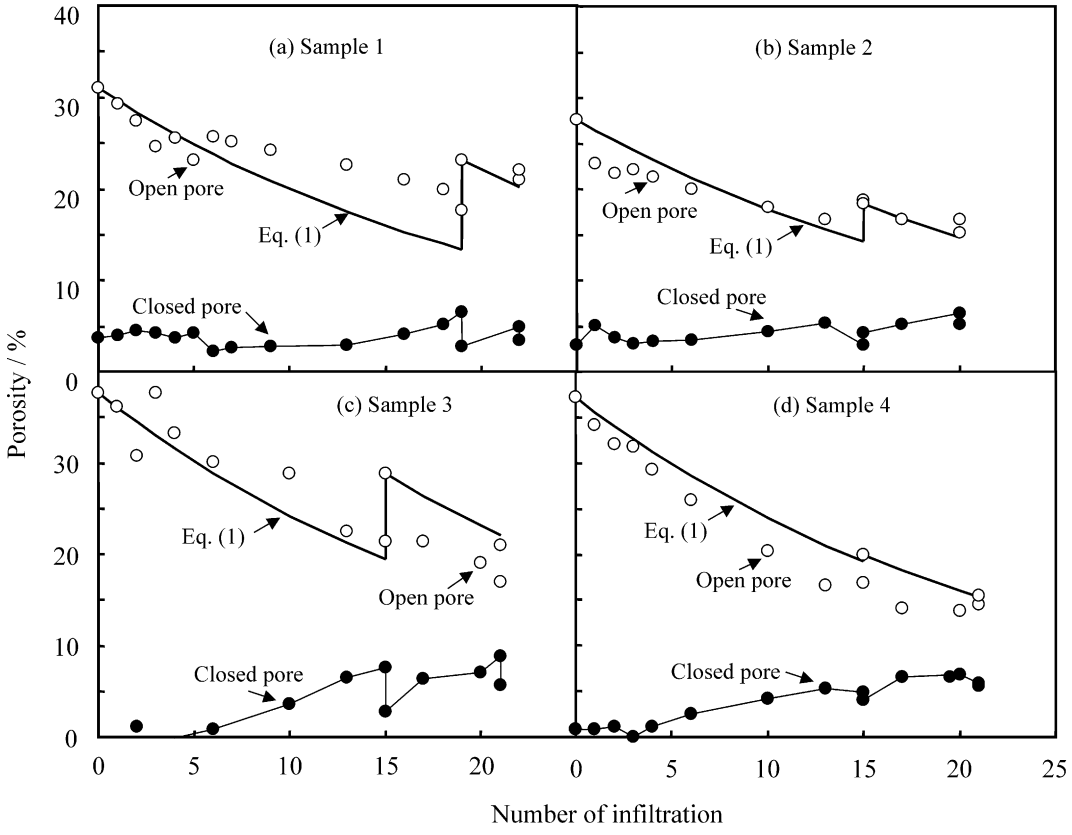

Fig. 9. Porosity of the laminated composites as a function of the number of PIP sequence. The solid lines represent the porosity calculated by Eq. (1) in text. See Table 2 for samples.

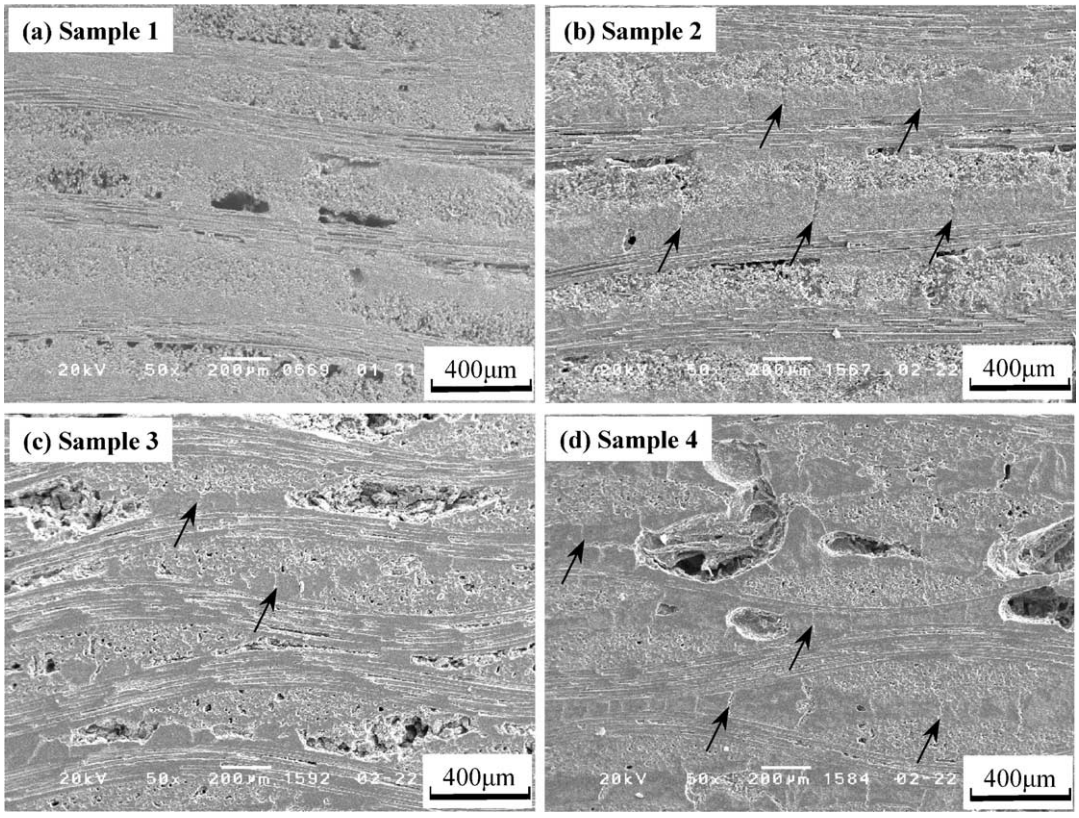

Fig. 10. Cross section of the densified composites after 20–23rd PIP sequence. The arrows in the microphotographs show the cracks in the matrix prepared from the mullite precursor.

dense uniform microstructure is the use of a low viscosity aqueous mullite suspension of a high content of well dispersed mullite filler during the lamination of the woven satin or fabric. After the 20–23rd PIP process, no cracks were observed in the matrix of sample 1 with SiC satin. However, some cracks, indicated by the arrows in Fig. 10, were formed in the matrix of samples 2, 3 and 4 with aluminosilicate fabric. The cracks were formed by the nonuniform distribution of the tensile stress in the matrix during the PIP process with the mullite precursor. The relatively strong adhesion between the mullite filler and the aluminosilicate fabric caused by the mullite precursor may suppress the relaxation of the stress produced during densification in the PIP process. The low affinity of SiC fiber for the mullite precursor reduces the nonuniformity of the stress distribution in the mullite matrix.

3.4. Mechanical properties of the densified composites

Fig. 11 shows typical stress–displacement curves for the laminated composites. Samples 1 and 2 showed elastic deformation in the initial stage of the stress–displacement curves, followed by significant pseudoductility. The photographs shown in Fig. 12 correspond to the appearance of sample 1 at the displacements indicated by the arrows in Fig. 11. After the elastic deformation (point 1), sample 1 gradually deformed like a metal and still maintained its original shape at over 1 mm displacement (point 5). This deformation behavior is based on the remarkable delamination of the layered SiC satin [Fig. 13(a)]. In sample 2, a similar delamination of the layered aluminosilicate fabric was observed in the fractured surface [Fig. 13(b)]. On the other hand, samples 3 and 4 fractured catastrophically with no pseudoductility. Fig. 13(c) and (d) show the fracture surface of samples 3 and 4. Little pullout of the aluminosilicate fibers or no delamination of the fabric was observed, resulting in the brittle fracture. Table 3 summarizes the mechanical properties of the SiC satin or aluminosilicate fabric-reinforced mullite matrix composites. The maximum deformation strength was 83 ± 11, 52 ± 15, 37 ± 11 and 47 ± 13 MPa for samples 1, 2, 3 and 4, respectively. The fracture energy at 1.5 mm of displacement was 4.2 ± 0.5 and 1.2 ± 0.4 kJ/m^2 for samples 1 and 2, respectively. Table 3 also compares the mechanical properties of CFCCs. The flexural strength is influenced by the relative density of the composites rather than the types of CFCCs. Sample A (nonoxide/nonoxide),[47] sample B (nonoxide/nonoxide & oxide)[39] and sample D (oxide/oxide)[13] with 90–93% density provided the high flexural strength of 260–470 MPa. The relatively low strengths of CFCCs prepared in this experiment (samples 1 and 2) are due to the high por-

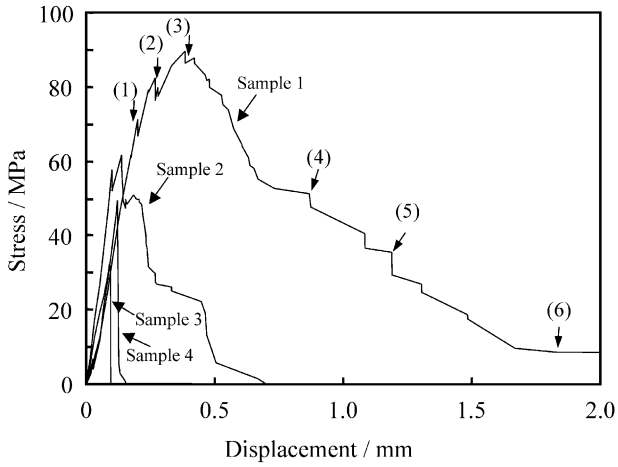

Fig. 11. Stress–displacement curves for the laminated composites with SiC satin (sample 1) and aluminosilicate fabric (samples 2–4). See Tables 2 and 3 for samples.

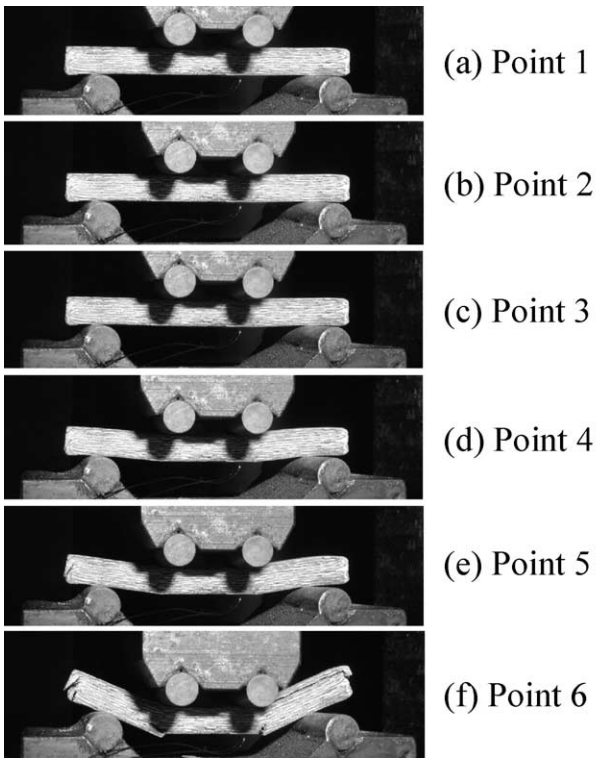

Fig. 12. Appearance of sample 1 at the displacement indicated by the arrows in Fig. 11.

osity (22–25%). Further densification may be effective to increase the strength. On the other hand, the fracture energy is strongly associated with the pseudoductility. The fracture energy measured in this experiment (samples 1 and 2) was comparable to that measured for the dense composites with high strengths (samples A and D). As seen in Table 3, the PIP process gave the advantage of high fracture energy without the formation of interphase on the fibers.

The fracture behavior shown in Fig. 11 is associated with the microstructure as follows. Samples 1 and 2 contained a large amount of mullite filler in the yarn of the laminated fabric (Table 2). No sintering occurs between the mullite particles during the low temperature PIP process (500–1000 °C). The infiltrated mullite precursor, whose amount was relatively low (Table 2), may produce a chemical bond between the mullite particles or between the mullite particles and the laminated fabric after the pyrolysis. The adhesion strength of the mullite precursor-derived solid to the SiC fibers would be weaker than that to the aluminosilicate fibers because of the low chemical affinity between SiC and mullite. That

Table 3
Mechanical properties of ceramic fiber-reinforced ceramic materix composities

Sample [Ref.]	Fiber	Interphase	Matrix	Method	Fiber fraction (vol.%)	Relative density (%)	Mechanical properties	
							Flexural strength (MPa)	Fracture energy (kJ m^{-2})
A[47]	SiC (0.5 mass%O) (fabric)	BN	SiC	Slurry impregnation and RS	30	93	466	6.4
B[39]	Si–Ti–C–O (12 mass%O) (fabric)	–	Mullite filler and SiC	Slurry impregnation and PIP	35–37	90	290	11.4
No. 1 (This work)	SiC (0.5 mass%O) (satin)	–	Mullite filler and mullite precursor	Slurry impregnation and PIP	22	75	74–94	3.7–4.7[a]
No.2 (This work)	Aluminosilicate ($85Al_2O_3$–$15SiO_2$, mass%) (fabric)	–	Mullite filler and mullite precursor	Slurry impregnation and PIP	33	78	36–62	0.8–1.9[a]
C[15]	Aluminosilicate ($85A1_2O_3$–$15SiO_2$, mass%) (unidirectional)	Fugitive (oxidation of C)	CaO– Al_2O_3–SiO_2 glass	Hot-pressing	30–35	90–95	92 (tensile)	–
D[13]	Aluminosilicate ($70Al_2O_3$–$28SiO_2$–$2B_2O_3$, mass%) (unidirectional)	BN	Mullite	Hot-pressing	41	90	258	1.6

[a] Deformation energy at 1.5 mm of displacement.

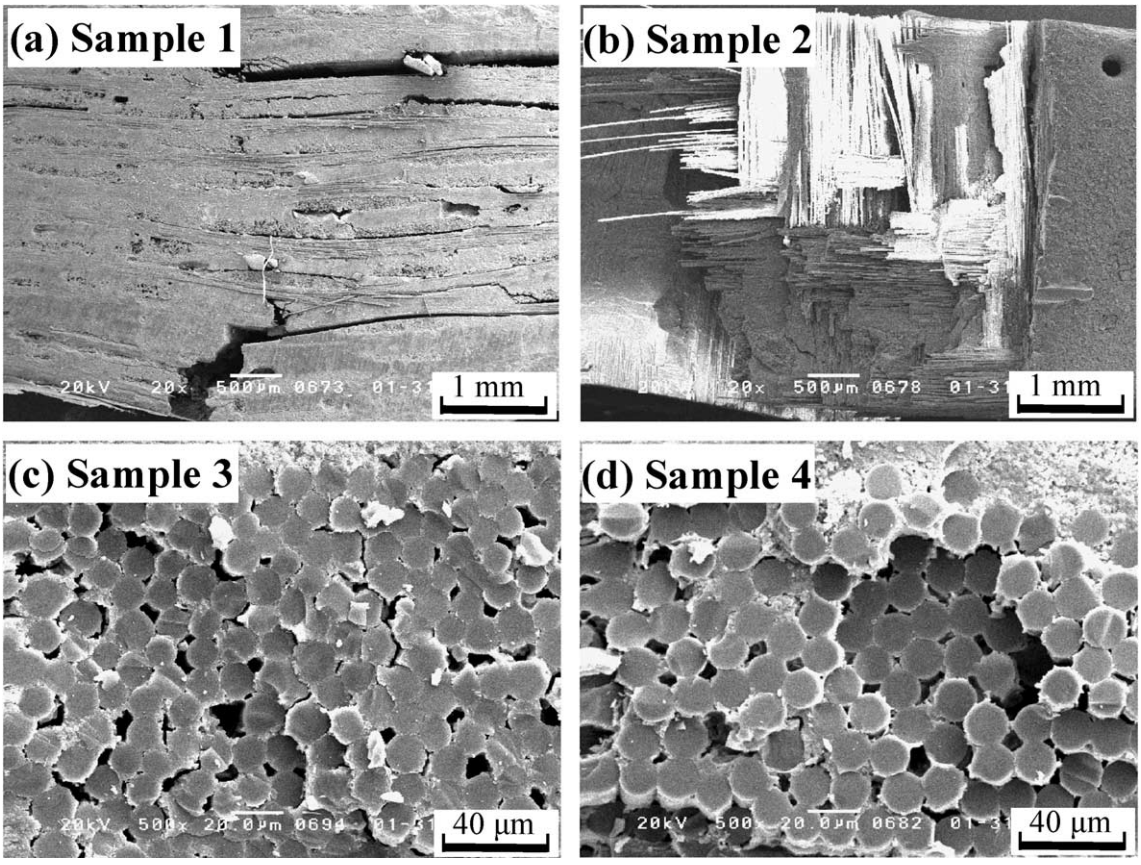

Fig. 13. Appearance of the fractured samples 1 (a) and 2 (b), and the cross section of samples 3 (c) and 4 (d) showing little pullout of aluminosilicate fibers.

is, the separation of fibers through the dispersed mullite particles [Fig. 14(a) and (b)] and the formation of a weak bond in the yarn by a small amount of amorphous solid from the mullite precursor, enables the laminated composite to undergo delamination.

On the other hand, the amount of mullite filler in the yarn was small in sample 3. In sample 4, the mullite filler formed particle clusters between the fiber yarn because of the low dispersibility of the mullite particles in the precursor solution [Fig. 8(d)]. As a result, little mullite filler was dispersed in the fiber yarn, causing direct contact between the aluminosilicate fibers [Fig. 13(c), (d)]. In addition, the amount of the mullite precursor-derived solid was greater in samples 3 and 4 than in samples 1 and 2. The mullite precursor infiltrated into samples 3 and 4 combined with the fibers in the yarn [Fig. 13(c) and (d)], resulting in the loss of flexibility. Therefore, the nonuniform distribution of mullite filler between the yarn, the small amount of mullite filler in the yarn and the large amount of mullite precursor combined to form a relatively strong bond between the fibers in the yarn and thus prevented delamination.

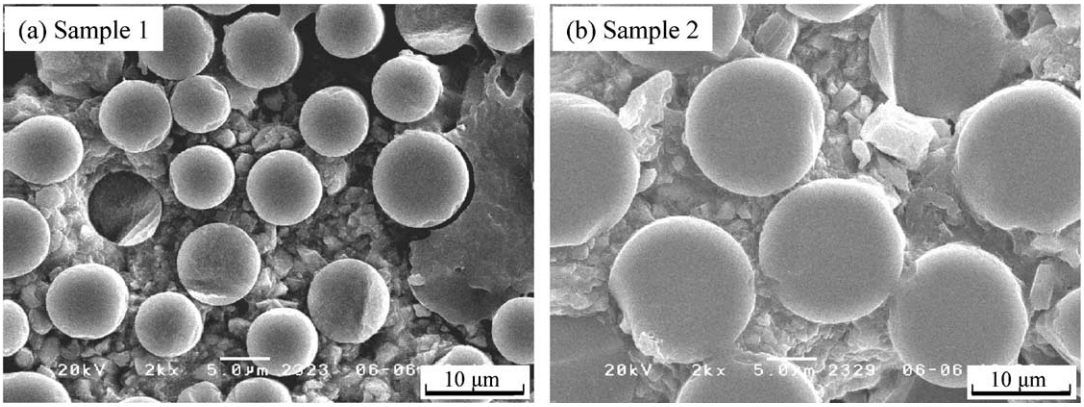

Fig. 14. Cross section of samples 1 (a) and 2 (b) showing the separation of fibers through the dispersed mullite particles.

4. Conclusions

(1) The amount of mullite filler in the green laminate of woven fabric or satin depended mainly on the mullite filler content of the aqueous suspension or of the mullite precursor suspensions ($Al(NO_3)_3$ plus $Si(OC_2H_5)_4$). However, the microstructure of the calcined composite was influenced by the dispersibility of the mullite particles in the suspension and by the viscosity of the suspension.

(2) The microstructure of the densified composites inherited the character of the green microstructure before the PIP process. The key factor to achieve a dense uniform microstructure is the use of a low viscosity aqueous mullite suspension with a large amount of well dispersed mullite filler during the lamination of the woven fabric.

(3) The separation of fibers in the yarn by the dispersed mullite particles and the formation of weak bonding in the yarn as a result of the small amount of amorphous solid from the mullite precursor, enabled the laminated composite to undergo pseudoductility with delamination.

(4) The nonuniform distribution of mullite filler between the yarn and the large amount of mullite precursor coupled to form relatively strong bonding between the fibers in the yarn, resulting in brittle fracture.

References

1. Kerans, R. J. and Parthasarathy, T. A., Crack deflection in ceramic composites and fiber coating design criteria. *Composites, Part A*, 1999, **30**, 521–524.
2. Kerans, R. J., Hay, R. S. and Pagano, N. J., The role of the fiber–matrix interface in ceramic composites. *Am. Ceram. Soc. Bull.*, 1989, **68**(2), 429–442.
3. Evans, A. G. and Zok, F. W., Review the physics and mechanics of fiber-reinforced brittle matrix composites. *J. Mater. Sci.*, 1994, **29**, 3857–3896.
4. Davis, J. B., Lofvander, J. P. A. and Evans, A. G., Fiber coating concepts for brittle-matrix composites. *J. Am. Ceram. Soc.*, 1993, **76**(5), 1249–1257.
5. Evans, A. G., Zok, F. W. and Davis, J. B., The role of interface in fiber-reinforced brittle matrix composites. *Composites Science and Technology*, 1991, **42**, 3–24.
6. Pagano, N. J., On the micromechanical failure model in a class of ideal brittle matrix composites part 1. Coated-fiber composites. *Composites, Part B*, 1998, **29B**, 93–119.
7. Pagano, N. J., On the micromechanical failure model in a class of ideal brittle matrix composites part 2. Uncoated-fiber composites. *Composites, Part B*, 1998, **29B**, 121–130.
8. Marshall, D. B. and Evans, A. G., Failure mechanisms in ceramic-fiber/ceramic-matrix composites. *J. Am. Ceram. Soc.*, 1985, **68**(5), 225–231.
9. Evans, A. G., He, M. Y. and Hutchinson, J. W., Interface debonding and fiber cracking in brittle matrix composites. *J. Am. Ceram. Soc.*, 1989, **72**(12), 2300–2303.
10. Thouless, M. D., Sbaizero, O., Sigl, L. S. and Evans, A. G., Effect of interface mechanical properties on pull out in a SiC-fiber-reinfoced lithium aluminum silicate glass ceramic. *J. Am. Ceram. Soc.*, 1989, **72**(4), 525–532.
11. Charalambides, P. G. and Evans, A. G., Debonding properties of residually stressed brittle matrix composite. *J. Am. Ceram. Soc.*, 1989, **72**(5), 746–753.
12. Llora, J. and Singh, R. N., Influence of fiber and interfacial properties on fracture behavior of fiber-reinforced ceramic composites. *J. Am. Ceram. Soc.*, 1991, **74**(11), 2882–2890.
13. Chawla, K. K., Xu, Z. R. and Ha, J.-S., Processing, structure, and properties of mullite fiber/mullite matrix composites. *J. Eur. Ceram. Soc.*, 1996, **16**, 293–299.
14. Yong, R. J. and Yang, X., Interfacial failure in ceramic fiber/glass composites. *Composites, Part A*, 1996, **27A**, 737–741.
15. Keller, K. A., Mah, T., Parthasarathy, T. A. and Cooke, C. M., Fugitive interfacial carbon coatings for oxide/oxide composites. *J. Am. Ceram. Soc.*, 2000, **83**(2), 329–336.
16. Bender, B., Shadwell, D., Bulik, C., Incorvati, L. and Lewis III, D., Effect of fiber coatings and composite processings on properties of ziroconia-based matrix SiC fiber composites. *Am. Ceram. Soc. Bull.*, 1986, **65**(2), 363–369.
17. Lewinsohn, C. A., Henager, C. H. Jr., Jones, R. H. and Eldridge, J. I., Measuring interphase recession by fiber push-in testing. *J. Am. Ceram. Soc.*, 2001, **84**(4), 866–868.
18. Boakye, E., Hay, R. S. and Petry, M. D., Continuous coating of oxide fiber tows using liquid precursors: monazite coatings on Nextel 720™. *J. Am. Ceram. Soc.*, 1999, **82**(9), 2321–2331.
19. Kuo, D.-H., Kriven, W. M. and Mackin, T. J., Control of interfacial properties through fiber coating monazite coatings in oxide/oxide composites. *J. Am. Ceram. Soc.*, 1997, **80**(12), 2987–2996.
20. Morgan, P. E. D. and Marshall, D. B., Functional interfaces for oxide/oxide composites. *Mater. Sci. Eng., A*, 1993, **A162**, 15–25.
21. Parthasarathy, T. A., Boakye, E., Cinibulk, M. and Petry, M. D., Fabrication and testing of oxide/oxide microcomposites with monazite and hibonite as interlayers. *J. Am. Ceram. Soc.*, 1999, **82**(12), 3575–3583.
22. Mawdsley, T. R., Kovar, D. and Halloran, J. W., Fracture behavior of alumina/monazite multilayer laminate. *J. Am. Ceram. Soc.*, 2000, **83**(4), 802–808.
23. Morgan, P. E. D. and Marshall, D. B., Ceramic composites of monazite and alumina. *J. Am. Ceram. Soc.*, 1995, **78**(6), 1553–1563.
24. Cain, M. G., Cain, R. L., Lewis, M. H. and Gent, J., In situ reaction rare-earth hexaaluminate interphases. *J. Am. Ceram. Soc.*, 1997, **80**(7), 1873–1876.
25. Cinibulk, M. K. and Hay, R. S., Textured magnetoplumbite fiber-matrix interphase derived from sol-gel fiber coatings. *J. Am. Ceram. Soc.*, 1996, **79**(5), 1233–1246.
26. Iyi, N., Takekawa, S. and Kimura, S., Crystal chemistry of hexaaluminates: β-alumina and magnetoplumbite structure. *J. Solid State Chemistry*, 1989, **83**, 8–9.
27. Parthasarathy, T. A., Boakye, E., Keller, K. A. and Hay, R. S., Evaluation of porous ZrO_2–SiO_2 and monazite coating using Nextel™ 720-fiber-reinforced Blackglass™ minicomposites. *J. Am. Ceram. Soc.*, 2001, **84**(7), 1526–1532.
28. Colomban, P., Bruneton, E., Langrange, J. L. and Mouchon, E., Sol-gel mullite matrix-SiC and mullite 2D woven fabric composites with or without zirconia coating interphase: elaboration and properties. *J. Eur. Ceram. Soc.*, 1996, **16**(2), 301–314.
29. Sudre, O., Razzell, A. G., Molliex, L. and Holmquist, M., Alumina single-crystal fiber reinforced alumina matrix for combustor tiles. *Ceram. Eng. Sci. Proc.*, 1998, **19**(4), 273–280.
30. Kerans, R. J. and Parthasarathy, T. A., Theoretical analysis of the fiber pullout and pushout tests. *J. Am. Ceram. Soc.*, 1991, **74**(7), 1585–1596.
31. Iero, P. D., Kerans, R. J. and Parthasarathy, T. A., Effect of interfacial roughness on the frictional stress mea-

sured using pushout tests. *J. Am. Ceram. Soc.*, 1991, **74**(11), 2793–2801.
32. Kerans, R. J., The role of coating compliance and fiber/matrix interfacial topography on debonding in ceramic composites. *Scr. Metall.*, 1995, **32**(4), 505–509.
33. Kerans, R. J., Viability of oxide fiber coatings in ceramic composites for accommodation of misfit stresses. *J. Am. Ceram. Soc.*, 1996, **79**(6), 1664–1668.
34. Parthasarathy, T. A., Barlage, D. R., Jero, P. D. and Kerans, R. J., Effect of interfacial roughness parameters on the fiber push out behavior of model composite. *J. Am. Ceram. Soc.*, 1994, **77**(12), 3232–3236.
35. Hirata, Y., Matsuda, M., Takeshima, K., Yamashita, R., Shibuya, M., Schmücker, M. and Schneider, H., Processing and mechanical properties of laminated composites of mullite/woven fabric of Si–Ti–C–O fibers. *J. Eur. Ceram. Soc.*, 1996, **16**(2), 315–320.
36. Li, J. X., Matsuo, Y. and Kimura, S., The role of fiber coating on SiC fiber-reinforced alumina composite. *J. Ceram. Soc. Jpn.*, 1992, **100**(4), 499–503.
37. Droillard, C. and Lamon, J., Fracture toughness of 2-D-woven SiC/SiC CVI-composites with multilayered interphases. *J. Am. Ceram. Soc.*, 1996, **79**(4), 849–858.
38. Jacobsen, T. K. and Brondsted, P., Mechanical properties of two plain-woven chemical vapor infiltrated silicon carbide-mattrix composites. *J. Am. Ceram. Soc.*, 2001, **84**(5), 1043–1051.
39. Hirata, Y., Matsura, T. and Hayata, K., Infiltration and pyrolysis of polytitanocarbosilane in a Si–Ti–C–O fabric/mullite porous composite. *J. Am. Ceram. Soc.*, 2000, **83**(5), 1044–1048.
40. Ogasawara, T., Ishikawa, T., Ito, H., Watanabe, N. and Davies, I. J., Multiple cracking and tensile behavior for an orthogonal 3-D woven Si–Ti–C–O fiber/Si–Ti–C–O matrix composite. *J. Am. Ceram. Soc.*, 2001, **84**(7), 1565–1574.
41. Guo, S. and Kagawa, Y., Temperature dependence of tensile strength for a woven boron-nitride-coated Hi-Nicalon^{TM} SiC fiber-reinforced silicon-carbide-matrix composite. *J. Am. Ceram. Soc.*, 1991, **74**(7), 1585–1596.
42. Morscher, G., Pirouz, P. and Heuer, A. H., Temperature dependence of interfacial shear strength in SiC-fiber-reinforced reaction-bonded silicon nitride. *J. Am. Ceram. Soc.*, 1990, **73**(3), 713–720.
43. Holz, D., Pagel, S., Bowen, C., Wu, S. and Claussen, N., Fabrication of low-to-zero shrinkage reaction bonded matrix composites. *J. Eur. Ceram. Soc.*, 1996, **16**(2), 255–260.
44. Aksay, I. A. and Pask, J. A., Stable and metastable equilibria in the system SiO_2–Al_2O_3. *J. Am. Ceram. Soc.*, 1975, **58**(11–12), 507–512.
45. Pugh R. J., In: *Surface and Colloid Chemistry in Advanced Ceramics Processing*, Ed. R. J. Pugh and L. Bergstom. Marcel Dekker, New York, 1994, pp. 127–192.
46. Hirata, Y., Dong, R., Yoshitomi, A., Hayata, K., Higashi, M. and Saegusa, K., Rheological properties and pressure filtration of In_2O_3–SnO_2 suspension. *J. Ceram. Soc. Japan*, 2001, **109**(1), 49–54.
47. Kameda, T., Sayano, A., Amiji, A., Ichikawa, H., Hamada, H., Fujita, A. and Uozumi, T., Fabrication and mechanical properties of reaction sintered silicon carbide matrix composite. *Ceram. Eng. Sci. Proc.*, 1997, **18**(3), 419–426.